ACS APPLIED MATERIALS & INTERFACES

Research Article

www.acsami.org

Thermomagnetic Processing of Liquid-Crystalline Epoxy Resins and Their Mechanical Characterization Using Nanoindentation

Yuzhan Li,[†] Orlando Rios,[‡] and Michael R. Kessler*,[†]

[†]School of Mechanical and Materials Engineering, Washington State University, P.O. Box 642920, Pullman, Washington 99164, United States

[‡]Materials Processing & Manufacturing Group, Oak Ridge National Laboratory, Oak Ridge, Tennessee 37831, United States

ABSTRACT: A thermomagnetic processing method was used to produce a biphenyl-based liquid-crystalline epoxy resin (LCER) with oriented liquid-crystalline (LC) domains. The orientation of the LCER was confirmed and quantified using two-dimensional X-ray diffraction. The effect of molecular alignment on the mechanical and thermomechanical properties of the LCER was investigated using nanoindentation and thermomechanical analysis, respectively. The effect of the orientation on the fracture behavior was also examined. The results showed that macroscopic orientation of the LC domains was achieved, resulting in an epoxy network with an anisotropic modulus, hardness, creep behavior, and thermal expansion.

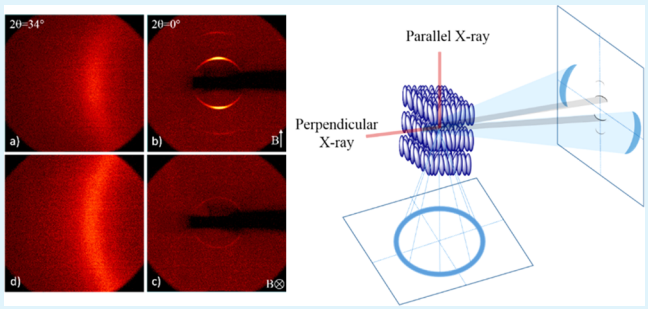

KEYWORDS: *liquid-crystalline epoxy resins, thermomagnetic processing, molecular orientation, mechanical properties*

1. INTRODUCTION

Thermomagnetic processing is an innovative technology that combines the application of magnetic fields with conventional high-frequency electromagnetic thermal processing. It allows customization of the structure of the material at microscale and nanoscale levels in order to tailor the properties and performance of the material. Thermomagnetic processing technology has been successfully used with alloys to selectively control the microstructure stability and phase-transformation kinetics.[1−3] Recent developments in the design and manufacturing of high-throughput thermomagnetic processing systems have been enabled by fully recondensing large warm bore superconducting magnets, transient field heating, and extraction systems.[4−6] However, the utilization of this technology with polymeric materials has not been fully explored and therefore remains an area of great potential to optimize the performance of polymeric materials. Oriented polymers often exhibit superior mechanical properties. For instance, carbon fibers owe their outstanding tensile properties to the highly oriented polyacrylonitrile crystallites during fiber spinning. Conversion of these polymer precursors under high magnetic fields has been shown to yield carbon fibers with enhanced alignment, leading to an improvement in the mechanical properties.[7] Therefore, the ability to control the molecular orientation of the polymer matrix in advanced composites is expected to enable unique mechanical, thermal, and electrical properties of structural and functional composites.

Low-molecular-weight thermotropic liquid crystals exhibit temperature-dependent phase behavior and show an active response to magnetic fields because of the molecular anisotropy of their diamagnetic susceptibility.[8] When these liquid-crystalline (LC) molecules are combined with the appropriate functional groups, they become reactive and can be polymerized into networks to retain their LC structure and molecular orientation.[9−15] Liquid-crystalline epoxy resins (LCER) are a special class of thermosetting polymers; they combine the characteristics of thermally reactive epoxies and magnetically responsive liquid crystals and are good candidates for thermomagnetic processing. LCERs are formed by curing rigid-rod epoxy monomers, which results in the retention of an LC phase in the amorphous networks. In the early stage of the curing reaction, the low viscosity allows control of the direction of the LC molecules through a magnetic field, so that the structure and properties of the resins can be tailored. Several research groups have studied the thermal and mechanical properties of oriented LCER networks using different techniques, including tensile testing and dynamic mechanical analysis.[16−18] However, the use of nanoindentation to investigate the orientation of such a material has not yet been reported.

Nanoindentation is a simple yet powerful tool to measure the mechanical properties of material samples with very small volumes.[19−23] The most widely used method to determine the elastic modulus and hardness for isotropic materials using nanoindentation was developed by Oliver and Pharr.[24] In recent years, this method has also been used with anisotropic materials and shown to be effective in evaluating their

Received: August 29, 2014
Accepted: October 8, 2014
Published: October 8, 2014

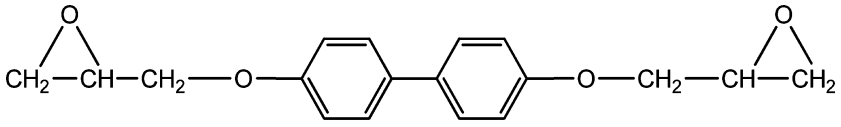

4,4'-Diglycidyloxybiphenyl (BP)

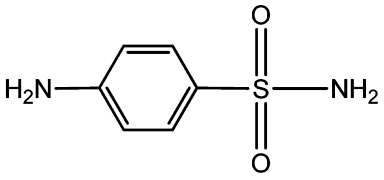

Sulfanilamide (SAA)

Figure 1. Chemical structures of the epoxy monomer and curing agent.

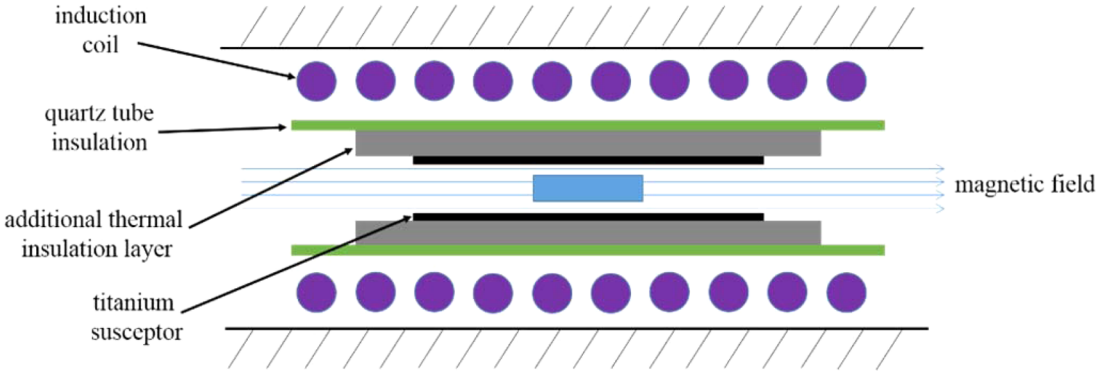

Figure 2. Schematic representation of the thermomagnetic processing system.

anisotropic mechanical behavior.[25−31] For example, Wang et al. investigated the elastic properties of a copper single crystal in the (111), (110), and (001) directions using nanoindentation and observed a significant difference in elastic moduli. Fan et al., on the other hand, used a three-dimensional finite elemental analysis (FEA) model to investigate the effects of anisotropy on nanoindentation measurements for cortical bone. It was found that the indentation moduli results calculated from the FEA simulation were similar to those obtained from nanoindentation experiments using the Oliver−Pharr method. Beake et al. studied the nanoindentation behavior of uniaxially and biaxially drawn poly(ethylene terephthalate) films and determined that the materials exhibited large differences in their mechanical properties caused by their processing histories.[32]

In the work reported herein, the use of thermomagnetic processing with a biphenyl-based LCER system was investigated. The structure of the oriented LCER was characterized using two-dimensional X-ray diffraction (2D-XRD), and it was correlated with mechanical and thermomechanical properties determined by nanoindentation tests and thermomechanical analysis.

2. EXPERIMENTAL DETAILS

2.1. Materials. Benzyltrimethylammonium bromide, 4,4′-dihydroxybiphenyl with 97% purity, and sulfanilamide (SAA) were purchased from Sigma-Aldrich (Milwaukee, WI). Epichlorohydrin with 99% purity was obtained from Acros Organics (Geel, Belgium). Sodium hydroxide, isopropyl alcohol, chloroform, methanol, and acetone were supplied by Fisher Scientific (Fair Lawn, NJ). All chemicals were used as received without further purification.

The epoxy monomer 4,4′-diglycidyloxybiphenyl (BP) was synthesized according to a procedure reported in an earlier work.[33] The chemical structures of the epoxy monomer and curing agent are shown in Figure 1. Previously, we examined the curing behavior of this system[34,35] and reported that the reaction between BP and SAA results in the formation of a smectic LC phase. The resulting resin showed a polydomain structure, with all LC domains randomly distributed in the amorphous network.

2.2. Thermomagnetic Processing. Thermomagnetic processing of the LCER was conducted at Oak Ridge National Laboratory using a superconducting magnet system, schematically shown in Figure 2. The magnetic field was created by coils of superconducting wires. A metallic susceptor was used as the heat source, converting electromagnetic energy into thermal energy, and therefore allows simultaneous curing and alignment of the LCER. Thermomagnetic processing was performed in a 9 T superconducting magnet with a 127-mm-diameter horizontal warm bore. Electromagnetic energy was supplied by a 9 kW power supply set to resonate at 175 kHz when coupled with an applicator. The thickness of the susceptor was 10 times the skin depth in order to shield the samples from the intense radio-frequency energy and to make sure they were heated only by radiant energy supplied uniformly by the tubular heating element. Thermomagnetic processing was performed using actively controlled thermal profiles that were designed to reproduce the transient conditions experienced by the samples. The alternating-current electromagnetic energy that was coupled to the susceptor was below 300 W during thermomagnetic processing.

In the experiment, the epoxy monomer was placed in a beaker and heated in an oil bath to 170 °C (the melting point of BP is 156 °C, and the melting point of SAA is 165 °C). After the monomer was fully

melted, the curing agent was added under a stoichiometric ratio, followed by vigorous stirring for approximately 45 s. The liquid mixture was poured into a poly(tetrafluoroethylene) mold and immediately transferred to the magnetic bore, which was preheated to 140 °C for alignment and curing. Because the reaction is highly exothermic, the preheating temperature of 140 °C was chosen to prevent overheating. After 10 min, the temperature was ramped to 170 °C at a rate of 2 °C/min. The oriented LCER was prepared by curing the sample under 9 T at 170 °C for 4 h. The unoriented LCER was prepared using the same procedure without a magnetic field.

2.3. Characterization. The structure and degree of orientation of the LCER were investigated using 2D-XRD. Diffraction patterns were collected using a Bruker D8 Advance diffractometer in transmission mode. The system was equipped with a HI-STAR area detector and controlled via Bruker software (*GADDS*, version 4.1.44). The X-ray source used in the experiments consisted of a chromium X-ray tube energized via a Kristalloflex 760 generator and maintained at 30 kV and 50 mA. A graphite monochromator was used to tune the source to Cr Kα radiation. In the experiment, a 0.8 mm collimator was used to control the divergence of the primary X-ray beam. A 6 × 4 mm specimen was mounted in the transmission fixture at a distance of 40 mm from the collimator assembly. A beam stop was placed 25 mm behind the test specimen. The detector was positioned 15 cm from the specimen. Data were collected by moving the detector in three individual increments (0°, 17°, and 34°) in the positive 2θ direction. A counting time of 300 s was used for each step. Data were corrected for spatial and flood field aberrations using the *GADDS* software.

The mechanical properties of the LCERs, cured both with and without a magnetic field, were studied using a Hysitron TI 900 nanoindentation system equipped with a Berkovich diamond indenter. A typical load−hold−unload cycle was used for indentation experiments, as shown in Figure 3. Once the indenter tip contacted the sample surface, the load was increased at a constant strain rate of 0.05 s^{-1} to 9.5 mN. Then the load was kept constant for 60 s to study the creep behavior of the resins. During the unloading phase, the indenter was withdrawn from the sample at a constant rate of 2 mN/s. A total of 25 indents were made on each sample, and the distance between each indent was 40 μm to avoid interactions.

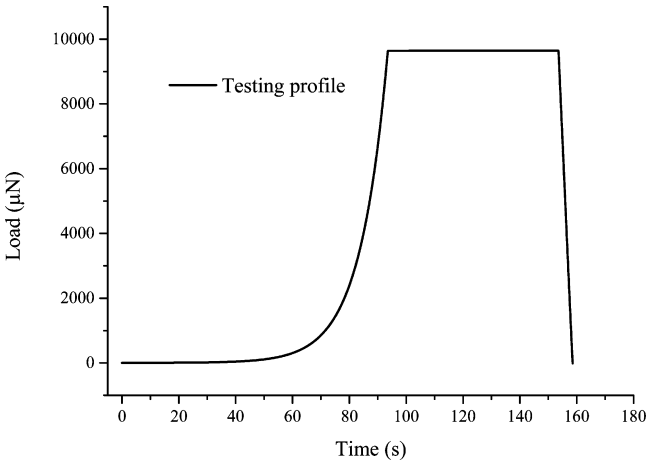

Figure 3. Testing profile used in the nanoindentation experiments.

The thermomechanical properties of the LCERs were studied by measuring the coefficient of thermal expansion (CTE) of the samples using a model Q400 thermomechanical analyzer (TA Instruments). The measurements were conducted in expansion mode with a heat−cool−heat cycle at 5 °C/min. The second heating scan was used to calculate the value of the CTE.

The fracture surfaces of the samples were examined using scanning electron microscopy (FEI Quanta 200F) to evaluate the effect of the LC orientation on the fracture morphology of the resin. Samples were sputter-coated with a layer of gold, and SEM images were collected at a 20 kV accelerating voltage.

3. RESULTS AND DISCUSSION

3.1. Orientation of the LCER. The orientation of the LCERs was characterized using 2D-XRD, which is widely used to study the preferred orientation in polymers.[36] In order to record high-resolution diffraction patterns of the smectic layer, the detector was set at 2θ = 0° to collect inner diffractions. The sample-to-film distance was chosen to be 15 cm. The detector was then moved to 2θ = 34° to collect outer diffractions. Two samples with different LC orientations were investigated, and the original 2D-XRD patterns are shown in Figure 4. The data were quantified by integration along the 2θ direction, and the results are shown in Figure 5.

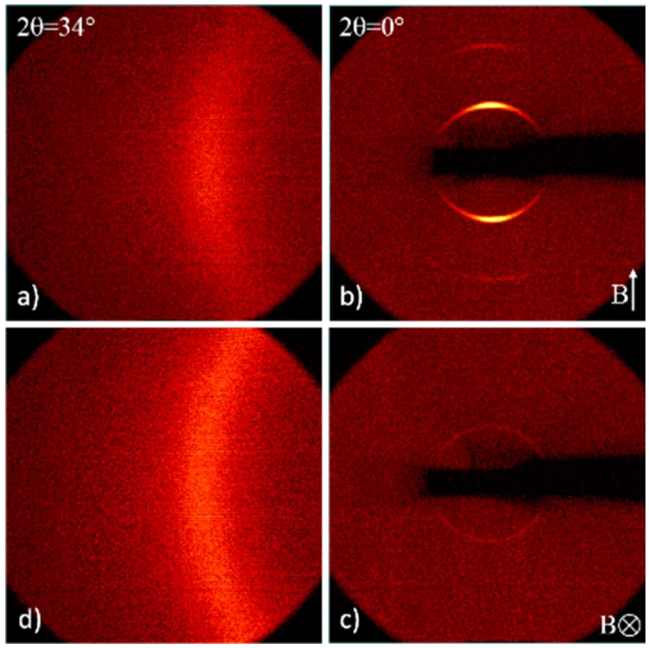

Figure 4. 2D-XRD patterns of oriented LCERs with different directions of the LC orientation: (a and b) incident X-ray beam perpendicular to the magnetic-field direction; (c and d) incident X-ray beam parallel to the magnetic-field direction.

The diffraction behavior was highly dependent on the sample orientation, indicating that macroscopic orientation of the LC domains had been achieved. For example, when the incident X-ray beam was perpendicular to the magnetic-field direction (Figure 4a,b), sharp diffraction arcs were observed in the meridional direction at a Bragg angle of 6.45°, caused by the layered smectic LC structure. The *d* spacing was calculated to be 20.3 Å according to Bragg's law. The value is quite close to the thickness of the smectic layer calculated from molecular simulation.[34] In addition, a second-order diffraction was observed at a Bragg angle of approximately 13°, suggesting that most of the smectic LC domains were oriented along the applied magnetic field. The samples also showed a diffraction arc in the equatorial direction at a Bragg angle of 29.5°, which corresponded to the diffraction from lateral-packed biphenyl mesogens. Because the mesogens within a smectic layer are less regulated, the diffraction arc appeared to be more diffuse compared to the diffraction by the smectic layer. On the other hand, when the X-ray beam was parallel to the field direction

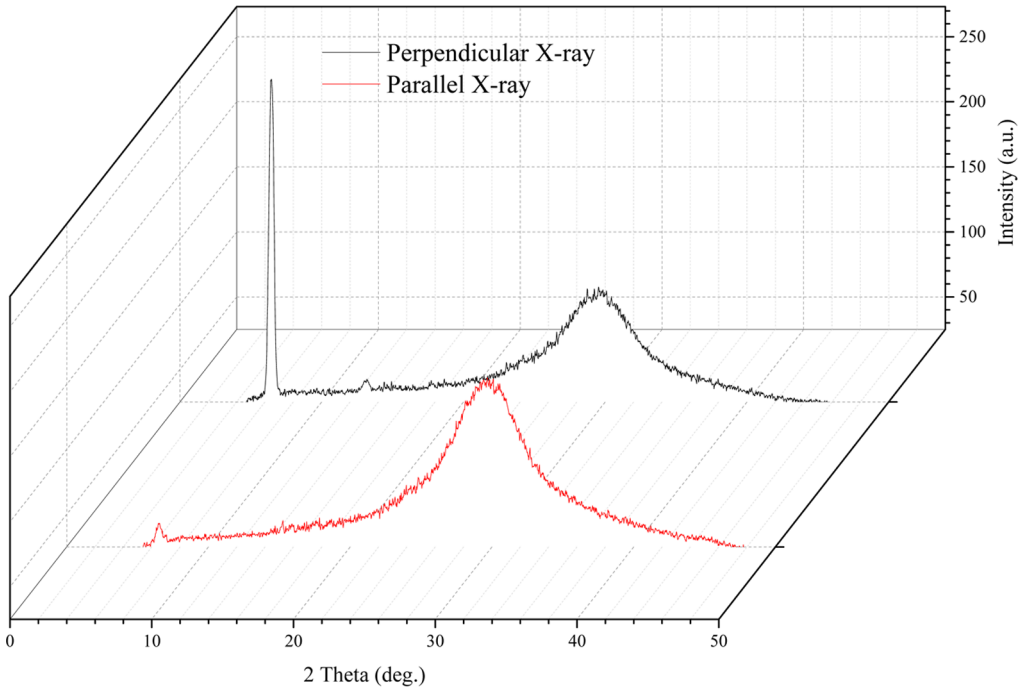

Figure 5. Quantified diffraction spectra after 2θ integration.

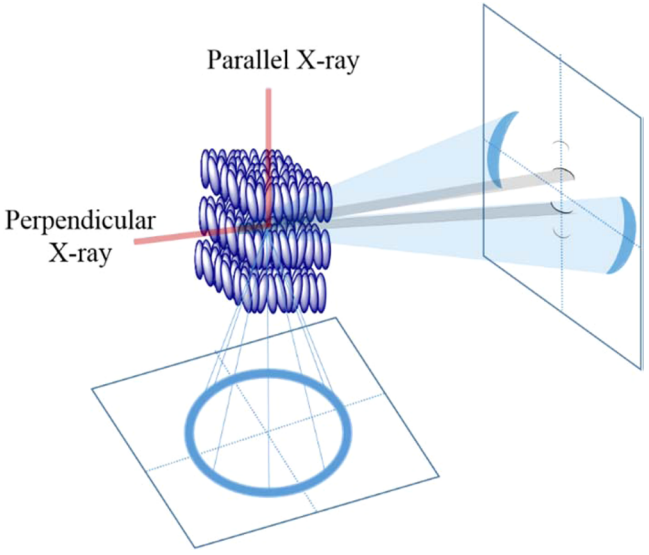

Figure 6. Schematic illustration of the diffraction patterns of a smectic LC domain.

(Figure 4c,d), a very weak diffraction ring was observed in the meridional direction. In the equatorial direction, a diffused diffraction ring was observed instead of a diffraction arc. Under such a configuration, the diffraction condition for the smectic layer was no longer satisfied, and the arrangement of the mesogens became effectively isotropic and showed a uniform intensity distribution in the diffraction pattern. An explanation for this behavior is schematically shown in Figure 6. It is worth mentioning that the *d*-spacing values of oriented LCERs were very close to those of unoriented LCERs, indicating that the application of the magnetic field only affected the direction and not the internal structure of the LC domains.

The degree of orientation of the LCER was evaluated based on the azimuthal intensity distribution of the inner diffraction arc from the smectic layer. An order parameter S was calculated according to Herman's method:[36]

$$S = \frac{1}{2}(3\langle \cos^2 \alpha \rangle - 1) \tag{1}$$

$$\langle \cos^2 \alpha \rangle = \frac{\int_0^{\pi/2} I(\alpha) \sin \alpha \cos^2 \alpha \, d\alpha}{\int_0^{\pi/2} I(\alpha) \sin \alpha \, d\alpha} \tag{2}$$

where α is the angle between the smectic layer normal and the magnetic field. $I(\alpha)$ is the intensity distribution of the sample; it can be directly calculated from the azimuthal intensity distribution of the diffraction arc. The degree of orientation of the LCER after thermomagnetic processing was determined to be 0.32, which was assumed to have a significant influence on the mechanical properties of the material.

3.2. Nanoindentation Behavior. The mechanical properties of the LCERs were studied using nanoindentation. For the sample prepared by thermomagnetic processing, the mechanical behavior, in both the longitudinal and transverse directions, was investigated and compared to that of unoriented LCERs. The load−displacement profiles of the samples are shown in Figure 7a−c, depicting the behavior of unoriented LCERs and of oriented LCERs in the longitudinal and transverse directions, respectively. The figure shows that the three samples exhibited different mechanical responses under the same loading profile, illustrating the influence of the molecular orientation on the mechanical properties of the resin. The load−displacement curves of unoriented LCERs were more consistent than those of oriented LCERs. This was attributed to the random orientation and distribution of the LC domains, which resulted in a material with isotropic and homogeneous properties. In the case of oriented LCERs, the use of a magnetic field caused macroscopic orientation. However, the orientation process was affected by several factors, such as thermal agitation of the LC molecules and the cross-linking reaction with the curing agent.

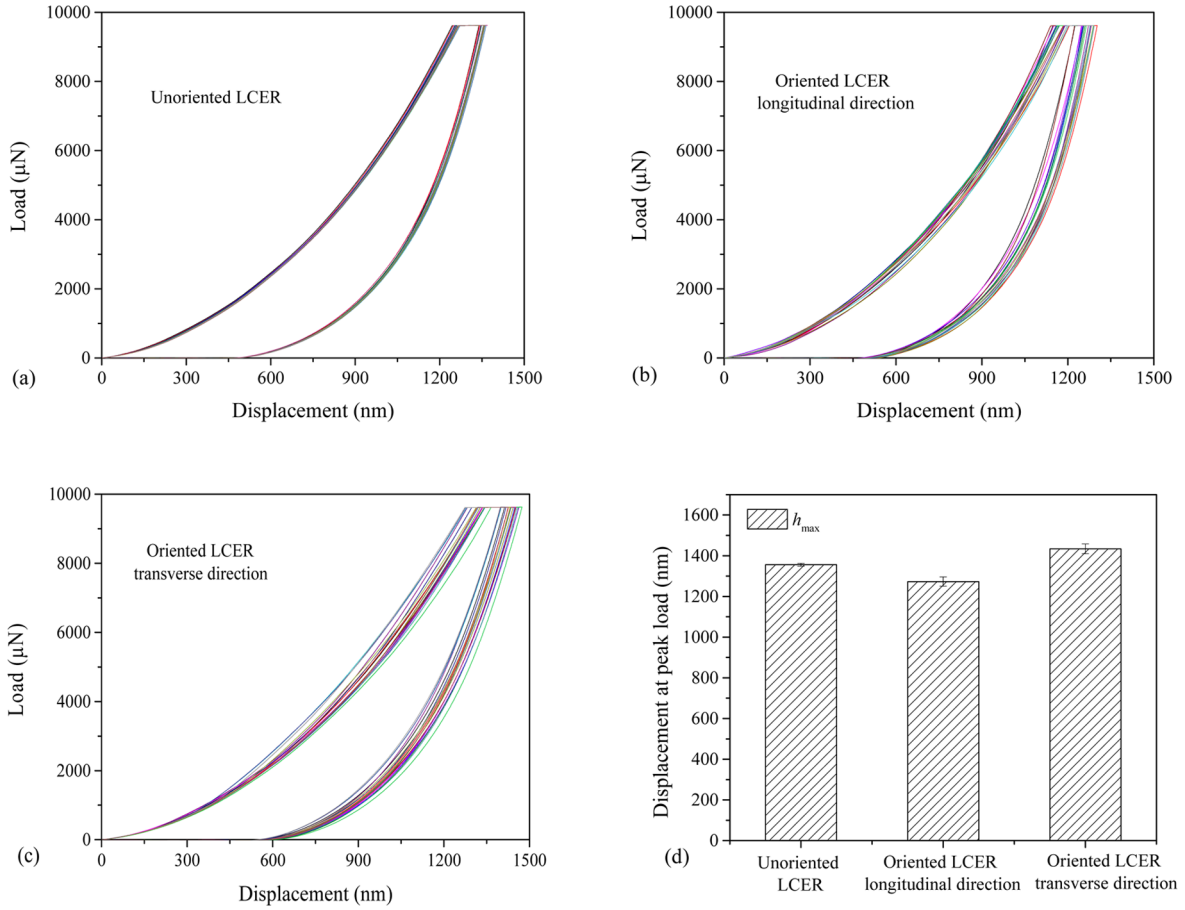

Figure 7. Load–displacement profiles and indentation displacement of LCER samples: (a) unoriented LCERs; (b) oriented LCERs in the longitudinal direction; (c) oriented LCERs in the transverse direction; (d) displacement of LCER samples at peak indentation load.

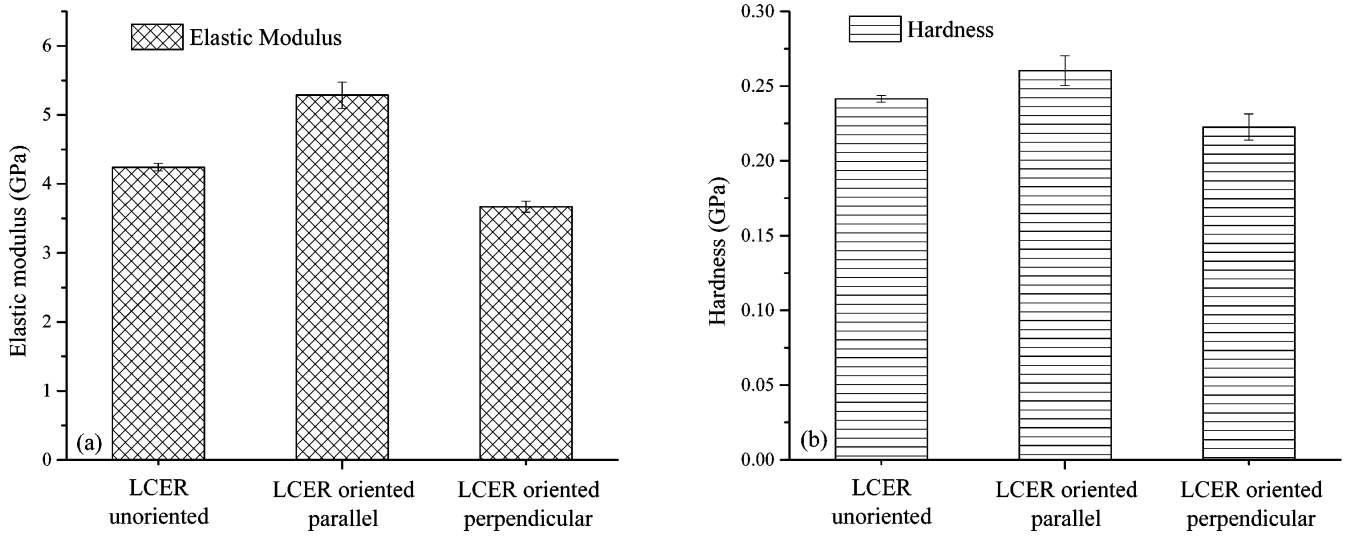

Figure 8. Effect of the LC orientation on the (a) modulus and (b) hardness of the LCERs.

Table 1. Mechanical Properties of the LCERs Determined by Nanoindentation Experiments

	maximum displacement (nm)	contact stiffness (μN/nm)	elastic modulus (GPa)	hardness (GPa)	average creep displacement
unoriented LCER	1355.4 ± 7.3	34.3 ± 0.3	4.242 ± 0.064	0.242 ± 0.002	93.33 ± 1.14
oriented LCER, longitudinal direction	1273.1 ± 22.9	41.1 ± 1.3	5.284 ± 0.192	0.260 ± 0.009	88.66 ± 6.98
oriented LCER, transverse direction	1433.9 ± 23.6	30.9 ± 0.7	3.669 ± 0.079	0.223 ± 0.009	115.10 ± 6.08

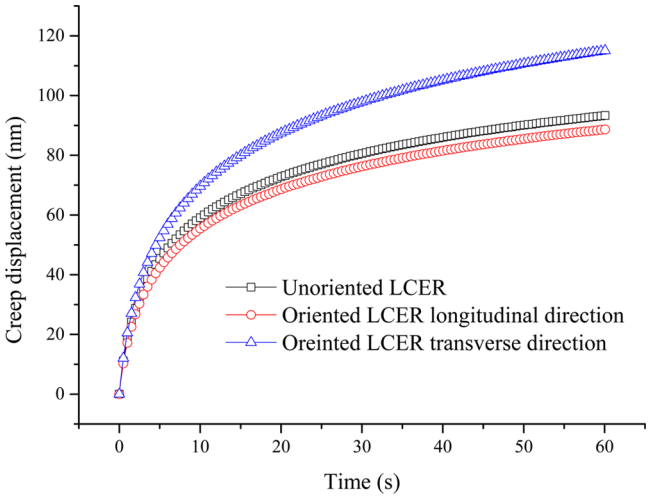

Figure 9. Effect of the LC orientation on the creep behavior of the LCERs.

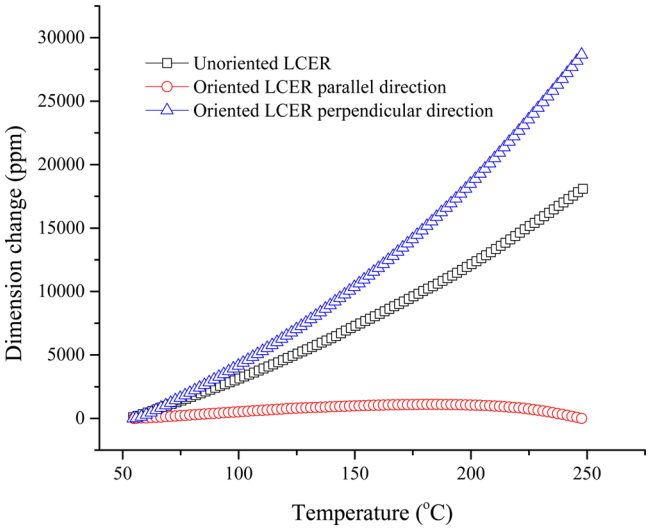

Figure 10. Effect of the LC orientation on thermal expansion of the LCERs.

Table 2. CTE Values of the LCERs Determined by Thermomechanical Analysis

	CTE (μm/°C)	
	glassy region	rubbery region
unoriented LCER	66.75	126.9
oriented LCER, longitudinal direction	12.11	−27.44
oriented LCER, transverse direction	92.74	217.7

The LC domains may not have been perfectly aligned along the field direction, and each domain may exhibit a different angle with respect to the magnetic-field direction. This localized inhomogeneity in terms of the LC orientation resulted in variation of the indentation behavior observed in Figure 7b,c.

An important parameter in nanoindentation experiments is the displacement at the peak load, h_{max}, which represents the resistance of a material to mechanical deformation. The displacement results for all samples are plotted in Figure 7d. Here the LCERs oriented in the longitudinal direction showed the lowest value of h_{max} under the same loading profile, indicating higher resistance to deformation in the direction of orientation. The existence of rigid and oriented LC domains attributed to this behavior will be further discussed in the next section.

A detailed analysis of the nanoindentation data was carried out according to a procedure developed by Oliver and Pharr,[24] fitting the unloading curves using a power-law equation:

$$P = \alpha(h - h_f)^m \tag{3}$$

where P is the indentation load, h is the displacement, and m and α are the fitting parameters. Then the contact stiffness (S) was determined from the initial slope of the unloading curve.

$$S = \frac{dP}{dh}(h = h_{max}) \tag{4}$$

The contact area (A) was determined using the shape function of the Berkovich indenter:

$$A(h_c) = 24.56h_c^2 + C_1h_c^1 + C_2h_c^{1/2} + \ldots + C_6h_c^{1/32} \tag{5}$$

where h_c is the contact depth. C_i values are parameters determined from calibration. The first term describes the contact area of a perfect Berkovich indenter; the others are correcting terms reflecting tip-blunting. The reduced elastic modulus was calculated and correlated to the sample modulus by the following equations:

$$E_r = \frac{1}{\beta}\frac{\sqrt{\pi}}{2}\frac{S}{A} \tag{6}$$

$$\frac{1}{E_r} = \frac{1-\nu_s^2}{E_s} + \frac{1-\nu_i^2}{E_i} \tag{7}$$

where E_i (1141 GPa) and ν_i (0.07) are the elastic modulus and Poisson's ratio for the diamond indenter. E_s and ν_s are the same properties for the sample. In this experiment, the Poisson's ratio of the resin was set to be 0.35 to calculate the elastic modulus.

The hardness of the sample was defined as the peak load divided by the contact area and calculated as

$$H = \frac{P_{max}}{A} \tag{8}$$

The elastic modulus and hardness of the LCERs are shown in Figure 8. After magnetic processing, the LCER exhibited anisotropic mechanical behavior. In the longitudinal direction, the resin showed an improvement of 24.6% in the elastic modulus and an improvement of 7.4% in the hardness compared to the unoriented LCER. In the transverse direction, however, the modulus and hardness of the oriented LCER showed decreases of 13.5% and 7.8%, respectively. These changes were closely related to the orientation of the LC molecules. As shown in Figure 6, the smectic LC domain consisted of laterally packed, layered biphenyl mesogens. The mesogens in different layers were covalently connected through SAA molecules, whereas the mesogens in the same layer were bonded by van der Waals forces such as π stacking. Therefore, the modulus and hardness of a single LC domain were expected to be anisotropic. In the unorinted LCER, the LC domains were randomly distributed and the anisotropy of the LC domains was neutralized. After magnetic processing, however, the original properties of the LC domains were retained and transferred from microscale to macroscale, resulting in a resin network with anisotropic mechanical behavior. Other mechan-

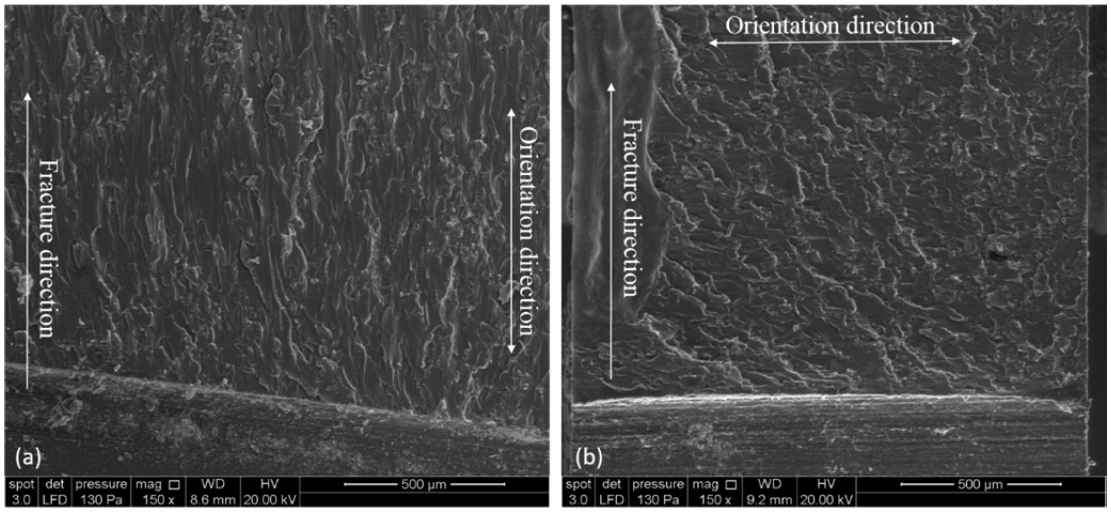

Figure 11. Effect of the LC orientation on the fracture morphologies of the LCERs: (a) fracture direction parallel to the LC orientation; (b) fracture direction perpendicular to the LC orientation.

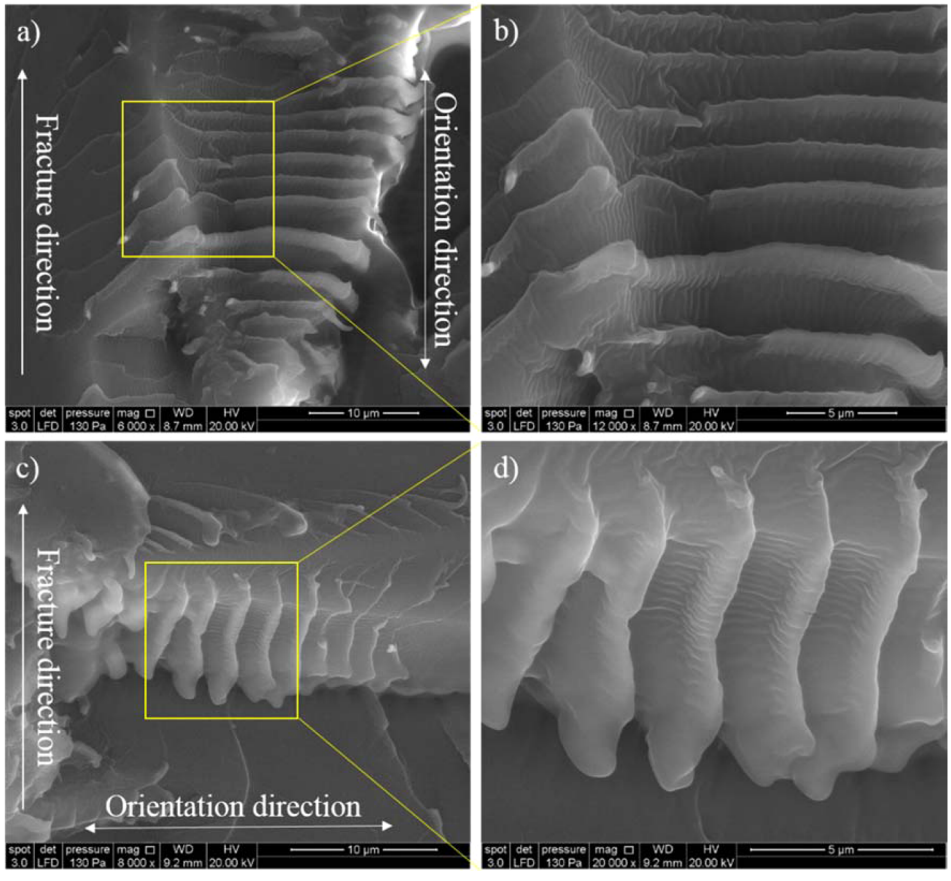

Figure 12. Effect of the LC orientation on the fracture morphologies of the LCERs: (a and b) fracture direction parallel to the LC orientation; (c and d) fracture direction perpendicular to the LC orientation.

ical properties investigated using the nanoindentation tests are summarized in Table 1.

The effect of the LC orientation on the viscoelastic properties of LCERs was investigated by studying their creep behavior. The resins were deformed under a constant load of 9.5 mN for 60 s after the initial loading. The creep displacements of the samples are shown in Figure 9. Similar to the results for the modulus and hardness, anisotropic creep behavior was observed for the LCERs after orientation. A decrease of 5% in creep displacement in the longitudinal direction and an increase of 23% in the transverse direction compared to the LCER with random orientation were observed. In a previous investigation, the creep performance of this LCER was studied and compared with the same resin cured into an amorphous phase.[37] The resin showed an improvement in the creep resistance after incorporation of the

LC domains, even when they were randomly oriented. As shown in Figure 9, this resistance can be further improved through magnetic processing.

3.3. Thermal Expansion. The magnetic orientation also significantly affected the thermomechanical properties of the resins. The CTE values of the LCERs were measured using thermomechanical analysis, and the results are shown in Figure 10 and Table 2. In the glassy region (60−80 °C), the oriented LCER exhibited a CTE value of 12.11 μm/°C in the longitudinal direction and a CTE value of 92.74 μm/°C in the transverse direction. This effect was also attributed to the structure and orientation of the LC domains. In the direction of orientation, thermal expansion was highly restricted by the rigid, covalently bonded LC mesogens, whereas in the transverse direction, the van der Waals forces were less effective in holding the mesogens together. Interestingly, in the rubbery region (220−240 °C), a negative CTE value was observed for the oriented LCER in the longitudinal direction. Similar behavior was observed for highly oriented fibers, such as Kevlar, which also showed strong covalent bonding in the longitudinal direction and weak bonding through van der Waals forces in the transverse direction.

3.4. Fracture Behavior. As discussed in the previous section, the mesogens within a smectic layer were mainly connected by van der Waals forces, whereas the mesogens in different layers were connected through covalent bonds. Therefore, the fracture behavior of the resin was expected to be influenced by the LC orientation. As shown in Figure 11, the fracture morphology of the resin was highly dependent on the fracture direction. When the resin was fractured in the direction perpendicular to its orientation direction (Figure 11b), crack propagation was redirected and changed to the direction of orientation so that the propagating cracks had to overcome only relatively weak van der Waals bonds rather than primary covalent bonds.

In general, smectic LC phases exhibited layered structures. During the SEM experiments, several layered structures were observed on the fracture surface, as shown in Figure 12. These layers were stacked along the direction of orientation and were independent of the fracture direction. It was concluded that these layered structures were related to the oriented smectic LC domains after magnetic-field processing.

4. CONCLUSIONS

In this work, the thermomagnetic processing technology of LCER systems was investigated. XRD results showed that the LC domains were successfully oriented along the magnetic-field direction. An order parameter of 0.32 was achieved. The effect of the orientation on the mechanical properties of the LCERs was studied using nanoindentation. Compared to unoriented LCERs, oriented samples showed anisotropic mechanical behavior with improved modulus, hardness, stiffness, and creep resistance in the longitudinal direction. The alignment of the LC domains also resulted in an epoxy network with anisotropic thermal expansion.

AUTHOR INFORMATION

Corresponding Author

*E-mail: MichaelR.Kessler@wsu.edu. Phone (509) 335-8654.

Notes

The authors declare no competing financial interest.

ACKNOWLEDGMENTS

The authors thank Dr. Scott Schlorholtz at the Materials Analysis Research Laboratory at Iowa State University for his help with the XRD experiments and Dr. Amy Wo for the helpful discussion regarding the nanoindentation experiments. The authors also thank Dr. Valerie Lynch-Holm at the Franceschi Microscopy & Imaging Center at Washington State University. Research sponsored in part by the Critical Materials Institute, an Energy Innovation Hub funded by U.S. Department of Energy, Office of Energy Efficiency and Renewable Energy, and Advanced Manufacturing Office, under contract DE-AC05-00OR22725 with UT-Battelle, LLC. Support through the Air Force Office of Scientific Research (Award FA9550-12-1-0108) is gratefully acknowledged.

REFERENCES

(1) Ludtka, G. M.; Jaramillo, R. A.; Kisner, R. A.; Nicholson, D. M.; Wilgen, J. B.; Mackiewicz-Ludtka, G.; Kalu, P. N. In Situ Evidence of Enhanced Transformation Kinetics in a Medium Carbon Steel Due to a High Magnetic Field. *Scr. Mater.* **2004**, *51*, 171−174.

(2) Jaramillo, R. A.; Babu, S. S.; Ludtka, G. M.; Kisner, R. A.; Wilgen, J. B.; Mackiewicz-Ludtka, G.; Nicholson, D. M.; Kelly, S. M.; Murugananth, M.; Bhadeshia, H. K. D. H. Effect of 30t Magnetic Field on Transformations in a Novel Bainitic Steel. *Scr. Mater.* **2005**, *52*, 461−466.

(3) Nicholson, D. M. C.; Kisner, R. A.; Ludtka, G. M.; Sparks, C. J.; Petit, L.; Jaramillo, R.; Mackiewicz-Ludtka, G.; Wilgen, J. B.; Sheikh-Ali, A.; Kalu, P. N. The Effect of High Magnetic Field on Phase Stability in Fe−Ni. *J. Appl. Phys.* **2004**, *95*, 6580−6582.

(4) Ludtka, G. M.; Wilgen, J. B.; Kenik, E. A.; Parish, C. M.; Rios, O.; Rogers, H.; Manuel, M.; Kisner, R. A.; Watkins, T. R.; Murphy, B. L. *High Magnetic Field Processing—a Heat-Free Heat Treating Method*; Technical Report; U.S. Department of Energy: Washington, DC, 2012.

(5) Potter, A.; Fischer, B. Improvements of Si-Crystal Growing Processes for Pv Applying Strong Magnetic Fields. *InterPV* **2010**, 82−85.

(6) Ludtka, G. M.; Mackiewicz-Ludtka, G. Advanced Induction Heating Coupled with Magnetic Field Processing. *Ind. Heat* **2013**, *81*, 43−48.

(7) Sung, M.-G.; Kawabata, Y. Strengthening of Carbon Fibers by a Magnetic Field Imposed in the Stabilization and Carbonization Process. *Mater. Sci. Eng., A* **2008**, *488*, 247−251.

(8) Gennes, P. G. d.; Prost, J. *The Physics of Liquid Crystals*; Clarendon Press: Gloucestershire, U.K., 1995.

(9) Carfagna, C.; Amendola, E.; Giamberini, M. Liquid Crystalline Epoxy Based Thermosetting Polymers. *Prog. Polym. Sci.* **1997**, *22*, 1607−1647.

(10) Shiota, A.; Ober, C. K. Rigid Rod and Liquid Crystalline Thermosets. *Prog. Polym. Sci.* **1997**, *22*, 975−1000.

(11) Barclay, G. G.; Ober, C. K. Liquid-Crystalline and Rigid-Rod Networks. *Prog. Polym. Sci.* **1993**, *18*, 899−945.

(12) Korner, H.; Shiota, A.; Bunning, T. J.; Ober, C. K. Orientation-on-Demand Thin Films: Curing of Liquid Crystalline Networks in Ac Electric Fields. *Science* **1996**, *272*, 252−255.

(13) Barclay, G. G.; Ober, C. K.; Papathomas, K. I.; Wang, D. W. Liquid-Crystalline Epoxy Thermosets Based on Dihydroxymethylstilbene—Synthesis and Characterization. *J. Polym. Sci., Part A: Polym. Chem.* **1992**, *30*, 1831−1843.

(14) Shiota, A.; Ober, C. K. Orientation of Liquid Crystalline Epoxides under Ac Electric Fields. *Macromolecules* **1997**, *30*, 4278−4287.

(15) Barclay, G. G.; McNamee, S. G.; Ober, C. K.; Papathomas, K. I.; Wang, D. W. The Mechanical and Magnetic Alignment of Liquid-Crystalline Epoxy Thermosets. *J. Polym. Sci., Part A: Polym. Chem.* **1992**, *30*, 1845−1853.

(16) Tan, C. B.; Sun, H.; Fung, B. M.; Grady, B. P. Properties of Liquid Crystal Epoxy Thermosets Cured in a Magnetic Field. *Macromolecules* **2000**, *33*, 6249−6254.
(17) Benicewicz, B. C.; Smith, M. E.; Earls, J. D.; Priester, R. D.; Setz, S. M.; Duran, R. S.; Douglas, E. P. Magnetic Field Orientation of Liquid Crystalline Epoxy Thermosets. *Macromolecules* **1998**, *31*, 4730−4738.
(18) Jahromi, S.; Kuipers, W. A. G.; Norder, B.; Mijs, W. J. Liquid-Crystalline Epoxide Thermosets—Dynamic-Mechanical and Thermal-Properties. *Macromolecules* **1995**, *28*, 2201−2211.
(19) Fischer-Cripps, A. C. Critical Review of Analysis and Interpretation of Nanoindentation Test Data. *Surf. Coat. Technol.* **2006**, *200*, 4153−4165.
(20) Ngan, A. H. W.; Wang, H. T.; Tang, B.; Sze, K. Y. Correcting Power-Law Viscoelastic Effects in Elastic Modulus Measurement Using Depth-Sensing Indentation. *Int. J. Solids Struct.* **2005**, *42*, 1831−1846.
(21) Pharr, G. M. Measurement of Mechanical Properties by Ultra-Low Load Indentation. *Mater. Sci. Eng., A* **1998**, *253*, 151−159.
(22) Van Landingham, M. R.; Villarrubia, J. S.; Guthrie, W. F.; Meyers, G. F. Nanoindentation of Polymers: An Overview. *Macromol. Symp.* **2001**, *167*, 15−44.
(23) Briscoe, B. J.; Fiori, L.; Pelillo, E. Nano-Indentation of Polymeric Surfaces. *J. Phys. D: Appl. Phys.* **1998**, *31*, 2395.
(24) Oliver, W. C.; Pharr, G. M. An Improved Technique for Determining Hardness and Elastic Modulus Using Load and Displacement Sensing Indentation Experiments. *J. Mater. Res.* **1992**, *7*, 1564−1583.
(25) Fan, Z.; Rho, J. Y.; Swadener, J. G. Three-Dimensional Finite Element Analysis of the Effects of Anisotropy on Bone Mechanical Properties Measured by Nanoindentation. *J. Mater. Res.* **2004**, *19*, 114−123.
(26) Pfetzing-Micklich, J.; Somsen, C.; Dlouhy, A.; Begau, C.; Hartmaier, A.; Wagner, M. F. X.; Eggeler, G. On the Crystallographic Anisotropy of Nanoindentation in Pseudoelastic Niti. *Acta Mater.* **2013**, *61*, 602−616.
(27) Faurie, D.; Djemia, P.; Le Bourhis, E.; Renault, P. O.; Roussigné, Y.; Chérif, S. M.; Brenner, R.; Castelnau, O.; Patriarche, G.; Goudeau, P. Elastic Anisotropy of Polycrystalline Au Films: Modeling and Respective Contributions of X-Ray Diffraction, Nanoindentation and Brillouin Light Scattering. *Acta Mater.* **2010**, *58*, 4998−5008.
(28) Kiran, M. S. R. N.; Varughese, S.; Reddy, C. M.; Ramamurty, U.; Desiraju, G. R. Mechanical Anisotropy in Crystalline Saccharin: Nanoindentation Studies. *Cryst. Growth Des.* **2010**, *10*, 4650−4655.
(29) Wang, W.; Lu, K. Nanoindentation Measurement of Hardness and Modulus Anisotropy in Ni3al Single Crystals. *J. Mater. Res.* **2002**, *17*, 2314−2320.
(30) Wang, W.; Lu, K. Nanoindentation Study on Elastic and Plastic Anisotropies of Cu Single Crystals. *Philos. Mag.* **2006**, *86*, 5309−5320.
(31) Gross, T. S.; Timoshchuk, N.; Tsukrov, I. I.; Piat, R.; Reznik, B. On the Ability of Nanoindentation to Measure Anisotropic Elastic Constants of Pyrolytic Carbon. *J. Appl. Math. Mech.* **2013**, *93*, 301−312.
(32) Beake, B. D.; Leggett, G. J. Nanoindentation and Nanoscratch Testing of Uniaxially and Biaxially Drawn Poly(Ethylene Terephthalate) Film. *Polymer* **2002**, *43*, 319−327.
(33) Su, W. F. A.; Chen, K. C.; Tseng, S. Y. Effects of Chemical Structure Changes on Thermal, Mechanical, and Crystalline Properties of Rigid Rod Epoxy Resins. *J. Appl. Polym. Sci.* **2000**, *78*, 446−451.
(34) Li, Y. Z.; Badrinarayanan, P.; Kessler, M. R. Liquid Crystalline Epoxy Resin Based on Biphenyl Mesogen: Thermal Characterization. *Polymer* **2013**, *54*, 3017−3025.
(35) Li, Y.; Kessler, M. Cure Kinetics of Liquid Crystalline Epoxy Resins Based on Biphenyl Mesogen. *J. Therm. Anal. Calorim.* **2014**, *117*, 481−488.
(36) Alexander, L. E. *X-Ray Diffraction Methods in Polymer Science*; Wiley-Interscience: New York, 1969.
(37) Li, Y.; Kessler, M. R. Creep-Resistant Behavior of Self-Reinforcing Liquid Crystalline Epoxy Resins. *Polymer* **2014**, *55*, 2021−2027.